DOI 10.1007/s11094-024-03058-5
Pharmaceutical Chemistry Journal, Vol. 57, No. 10, January, 2024 (Russian Original Vol. 57, No. 10, October, 2023)

DRUG SYNTHESIS METHODS AND MANUFACTURING TECHNOLOGY

TERNARY SOLID DISPERSION OF CELECOXIB PRODUCED BY THE SOLVENT METHOD WITH IMPROVED SOLUBILITY AND DISSOLUTION PROPERTIES

Lang Liu,[1] Fenfen Ouyang,[1] Ting Li,[1] Min Wen,[1] Guodong Zha,[2] Libo Chen,[1] Xue Fu,[1] and Li qing Zhu[1,*]

Original article submitted November 14, 2022.

Celecoxib, the first cyclooxygenase-2 selective nonsteroidal anti-inflammatory drug, has a wide range of pharmacological effects, including anti-inflammatory, antirheumatic and antitumor effects. However, celecoxib's poor solubility severely limits its clinical application. Thus, a novel ternary solid dispersion system was developed using PVP K30 and hydroxypropyl-β-cyclodextrin (HPβCD) as carrier materials in order to improve its solubility and dissolution behavior. The solid dispersion system was characterized by SEM, XRD, FT-IR, DSC, *in vitro* dissolution, saturated solubility, and contact angle test; the stability of the samples under extreme environments was investigated as well. The results showed that the novel ternary solid dispersion doped with PVP K30 and HPβCD has enhanced solubility around 6.28-fold, an almost 13.94-fold increase in the dissolution rate (120 min) compared with celecoxib's active pharmaceutical ingredient. The substantial improvement in its dissolution performance is attributed to the fact that celecoxib is dispersed in the carrier material in an amorphous form and has hydrogen bonding interactions with the carrier materials. In addition, the improvement of wettability is one of the reasons for its increased solubility. In conclusion, the combination of PVP K30 and HPβCD can significantly improve the solubility of celecoxib and this novel solid dispersion system provides new ideas and methods to further improve the solubility of insoluble drugs.

Keywords: celecoxib; solid dispersion; dissolution; co-carrier.

1. INTRODUCTION

Celecoxib (CXB) is a nonsteroidal anti-inflammatory drug (NSAID) for treating patients with rheumatism and osteoarthritis, which can lower gastrointestinal complication rates and cardiovascular side effects in clinical trials compared with earlier nonselective NSAIDs [1]. Celecoxib also has analgesic and anticancer properties, which are reported in the literature [1–6]. However, the poor water solubility and low bioavailability of CXB limit its clinical application [7–9]. To achieve the high drug solubility required to deliver therapeutic doses, there are several different enabling formulation strategies, including salt formation, complexation with cyclodextrins, self-emulsification, and solid dispersions (SDs), that have been selected for developing new CXB formulations [10–14]. The approach of SDs can provide one or more carrier materials, without involving chemical changes to the compound, and for some drugs, are often dispersed in carrier materials such as microcrystals, molecules, or amorphous forms [15]. Because an amorphous form has higher free energy than the crystalline counterparts, the oral delivery in the form of SDs is promising for poorly water-soluble drugs [14, 16 – 19].

In the current literature, the combination of hydrophilic polymers and surfactants was reported to give rise to higher solubility and subsequently bioavailability of CXB [20–22]. However, the potential toxicity of surfactants might be the main reason why their clinical application is limited [22, 23].

[1] Key Laboratory of Industrial Fermentation Microorganism, School of Chemistry and Chemical Engineering, Chongqing University of Science and Technology, Shapingba District, Chongqing 401331, People's Republic of China.
[2] Building #2, No.216, jianshan Road, Bishan District, Chongqing, China.
[*] e-mail: zhuliqing@cqust.edu.cn

Hydroxypropyl-β-cyclodextrin (HPβCD), which can enhance the water dispersion of hydrophobic compounds, has been extensively studied as a harmless excipient for preparing inclusion complexes [24, 25], but it has been less investigated for being a carrier material of SD. With the main goal of interpreting the solubilization mechanism of the ternary SD system, CXB was encapsulated into PVP K30 and HPβCD carrier materials by the rotary evaporation approach. In this study, characterization techniques such as scanning electron microscopy (SEM), x-ray diffractometry (XRD), Fourier transform infrared spectroscopy (FT-IR), differential scanning calorimetry (DSC), and a contact angle meter were used to detect and measure the ternary SD.

2. EXPERIMENTAL

2.1 Materials

Celecoxib was purchased from Wuhan Xinxin Beauty Biotechnology Co., Ltd. Povidone (PVP K30) and polyvinylpyrrolidone (PVP VA64), were a gift from Star-Tech & JRS Specialty Products Co., Ltd. Soluplus® was a gift from BASF, China. Hydroxypropyl-β-cyclodextrin was acquired from Shanghai Aladdin Bio-Chem Technology Co., Ltd. All solvents and chemicals were of analytical grade.

2.2 Methods

2.2.1 Phase solubility

Briefly, the excess amount of CXB was added and mixed in different HPβCD aqueous solutions, which were dissolved at different molar concentrations of 0, 10, 20, 30, 40, and 50 mmol/L. To measure the concentration of CXB by ultraviolet spectrophotometer (UV-1100, Shanghai Mapada Instrument Co., Ltd, China), the mixtures was placed in a shaking water bath apparatus (THZ-82, Hangzhou Jingfei Instrument Technology Co., Ltd., China) at 25°C at 200 rpm for 24 h, and then all the samples were immediately centrifuged at 12,000 rpm for 10 min. The supernatant was collected after centrifugation and diluted appropriately with filtering through 0.22-μm syringe filters.

2.2.2 Preparation of CXB-HPβCD inclusion complex

Ethanol was used to dissolve CXB; the solution had been stirred and mixed well to prepare a clear homogeneous solution; carrier material HPβCD was dissolved in purified water. The CXB-HPβCD inclusion complex was obtained by using a shaking water bath apparatus at 25°C at 200 rpm for 24 h, in which CXB was with HPβCD in a weight ratio of 1:4.04.

2.2.3 Preparation of binary solid dispersion

The carrier materials used in this study, such as PVP K30, PVP VA64, and Soluplus®, which was dissolved with ethanol, were mixed with CXB with a mass ratio of 3:1 respectively. The mixtures were magnet stirred for 6 h at room temperature (20–25°C). After the solution was completely transparent and homogenized, the rotary evaporator (Shanghai Yarong Biochemical Instrument Factory, China) was used to dry the mixtures at 120 rpm and 60°C. The samples were transferred into a petri dish and dried using the vacuum oven at room temperature (20–25°C) for 48 h, after grinding the SD in the agate mortar.

2.2.4 Optimized formulation of binary solid dispersions

To prepare binary SDs of CXB by singly using PVP K30, PVP VA64, and Soluplus® as the carriers, with dissolution in vitro was taken as the index. After the highest dissolution efficiency was obtained, we selected the optimal formulation of CXB binary SDs.

2.2.5 Preparation of ternary solid dispersions

The ternary SDs of CXB can be prepared as follows: the CXB-HPβCD inclusion complex containing 500 mg of CXB was uniformly mixed with the same mass of PVP K30, and dissolved in a beaker with a suitable amount of ethanol. Guided by the aforementioned experimental operation (2.2.3), after grinding SDs in the agate mortar, the acquired ternary SDs were stored in a desiccator for further use.

2.3 Characterization

2.3.1 x-ray diffractometry

Crystalline states of CXB active pharmaceutical ingredient (API), physical mixture (PM), and SDs were characterized by XRD by using a Shimadzu XRD-7000. Data were obtained in the range from 5° to 40° (2θ) at 5°/min with a step of 0.01°. Cu K_α radiation (40 kV, 30 mA) was used in all measurements.

2.3.2 Fourier transform infrared spectroscopy

The CXB API, PMs, and SDs were confirmed by FT-IR spectroscopy using a Bruker FT-IR spectrophotometer Tensor-27. Specimens were previously prepared using the potassium bromide (KBr) method at a wave number range from 4000 to 500 cm^{-1}. After comparing the infrared absorption characteristic of the specimens, the influence of API–excipient interactions were estimated.

2.3.3 Scanning electron microscopy

The size and morphology of CXB API, PMs, and SDs were investigated using a Sigma500 SEM (Zeiss, Ltd., Germany). After preparing a gold layer by vacuum deposition, the specimens were placed on the conductive adhesive tape, then SEM images were taken with an accelerating voltage of 5 kV.

2.3.4 Differential scanning calorimetry

A DSC 3+ (Mettler Toledo, Greifensee, Switzerland) was used to characterize the thermal properties of CXB API and

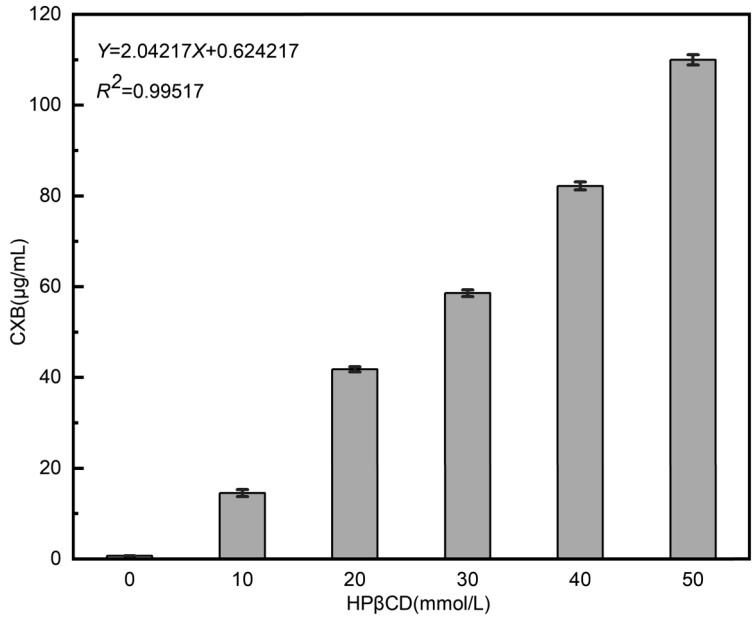

Fig. 1. Phase solubility profiles of celecoxib (CXB)/hydroxypropyl-β-cyclodextrin (HPβCD).

SDs. Specimens of 2 mg were placed in an aluminum crucible under nitrogen (50 mL/min) using a heating rate of 10°C/min from 30°C to 180°C.

2.3.5 Contact angle measurements

The contact angle of the compacted CXB, CXB-HPβCD, CXB-K30 SD, and CXB-K30-HPβCD SD were measured by the sessile drop method. The compacts with a 10-mm diameter and a weight of 200 mg were prepared with a compression force of 20 MPa for 30 sec. To test the contact angle, a drop of probe liquid (2 μL), pH 6.8 PBS buffer, was dispensed on tablets by injector.

2.3.6 Saturated solubility

Classical shake flask method was used for the saturated solubility test. Saturated solutions were prepared by adding 10 mL of PBS (pH 6.8) solution into each 30-mL volumetric flask, which contained an excess quantity of CXB API, PM, and SDs. The sparingly soluble specimens need to be shaken at 200 rpm and 37°C for 72 h to reach equilibrium. Then the specimens were filtered using cellulose filters with a 0.22-μm pore diameter. The amount of dissolved CXB was determined in triplicate by a Mapada UV-1100 ultraviolet spectrophotometer at 252 nm. The calibration curve ($A = 0.0544514C - 0.00144116$, $R^2 = 0.9993$) was used to calculate the saturated solubility of specimens in PBS.

2.3.7 In vitro dissolution

The *in vitro* drug release of samples was investigated by the second paddle method of dissolution in the Chinese Pharmacopoeia 2020 edition. The dissolution medium was 500 mL phosphate buffer solution (PBS, pH 6.8). CXB API, PM, and SDs (corresponding to 3 mg of celecoxib) were placed in dissolution vessels, as well as conducting at 37°C and 100 rpm. Aliquots (4 mL) of the medium was withdrawn from the vessels at predetermined time points (5, 15, 30, 45, 60, 90, and 120 min), and an equal volume of isothermic medium was replenished after each sampling. The collected samples were immediately filtered through a 0.22-μm syringe filter and replicated the measurement of CXB concentration in triplicate using an ultraviolet spectrophotometer.

2.4 Experiment on influencing factors

Guided by the Chinese Pharmacopoeia 2020 edition Part IV (9001), CXB SD was placed in weighing bottles for storing at 75% ± 1% relative humidity, the temperature at 60°C, and under simulated daylight irradiation with a light intensity of 4500 ± 500 lux respectively. Samples were withdrawn at intervals of 0, 5, and 10 days. The morphology characteristics, XRD characteristics, diffraction peaks, and dissolution behaviors of the samples were observed.

3. RESULTS AND DISCUSSION

3.1 Phase solubility study

Figure 1 displays the phase solubility diagrams of HPβCD in aqueous CXB solutions, which are classified according to Higuchi and Connors. CXB shows AL-type phase solubility profile. It illustrates that the solubility of CXB increased linearly with the increasing concentration of HPβCD, in case the 1:1 molar ratio inclusion was formed.

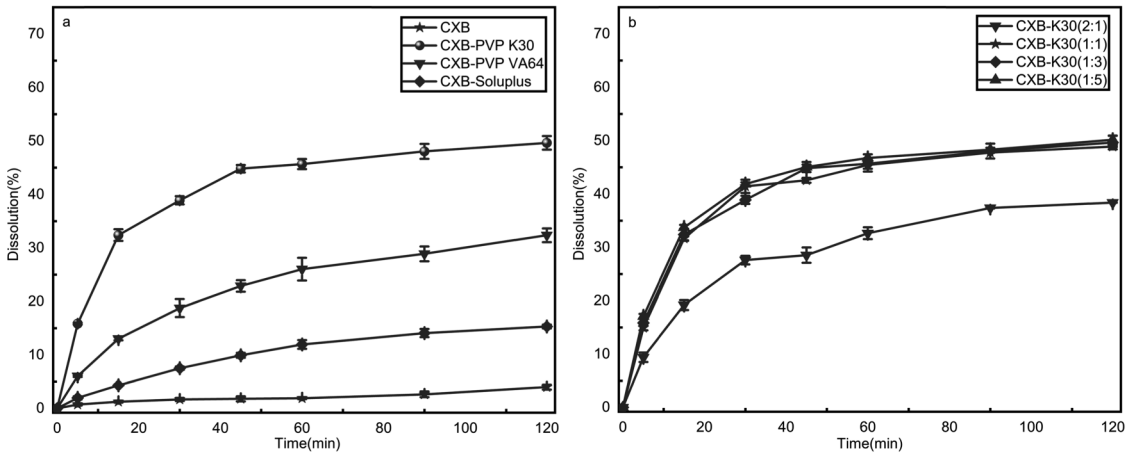

Fig. 2. Cumulative dissolution profiles of CXB and CXB binary SDs at 100 rpm; 37°C, medium volume 500 mL of (a) different carrier types and (b) different drug–carrier ratio. pH 6.8; mean ± SD; $n = 3$.

3.2 Screening of optimal binary solid dispersions

As shown in Fig. 2a, the carrier type and drug–carrier ratio of CXB binary SDs have been screened and optimized by dissolution rate in vitro. It is clearly demonstrated that the formation of binary SDs with PVP K30 carrier resulted in a substantial enhancement in the solubility of CXB. The highest drug release of 49.66% was obtained in 120 min, and pure CXB showed only 3.99%. With CXB–PVP VA64 and CXB–Soluplus® for binary SDs formulations, 32.37% and 15.32% in vitro dissolution were observed at 120 min respectively. Based on these data, the presence of PVP K30 can enhance solubilization of CXB–PVP K30 SD in pH 6.8 phosphate buffer. In consequence, PVP K30 should be used as a carrier to ensure the preparation of SDs, and simultaneously to conduct the optimization of the drug–carrier ratio.

The data in Fig. 2b show that a high dose of PVP K30 would increase the in vitro dissolution of CXB–PVP K30 SD in the pH 6.8 buffer; this result was consistent with those reported elsewhere [26]. With a 2:1 drug–carrier ratio of CXB–PVP K30 SD formulation, a 9.62-fold increase in drug release at the end of 120 min was observed, when compared with pure CXB API. With 1:1, 1:3, and 1:5 drug–carrier ratios of CXB–PVP K30 SD formulation, 12.25-fold, 12.44-fold, and 12.57-fold increases in drug release at the end of 120 min were observed respectively, compared with pure CXB API. Drug release obtained from 1:1, 1:3, and 1:5 drug–carrier ratios were 48.88%, 49.66%, and 50.17%,

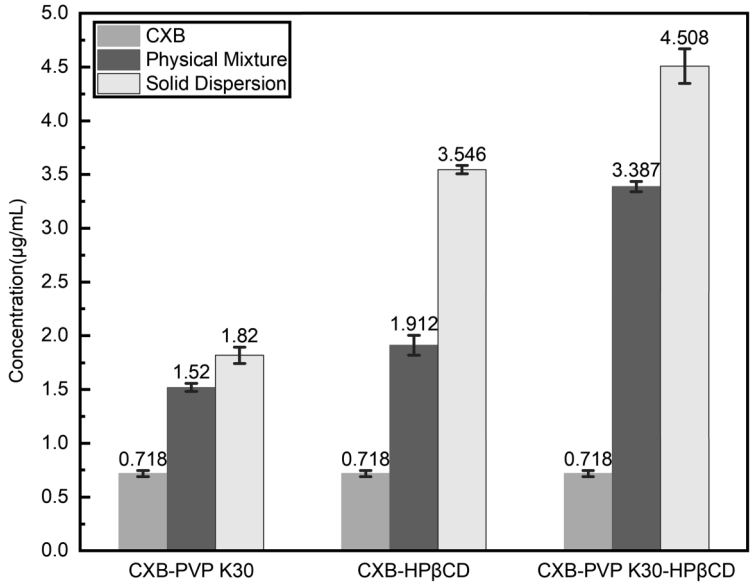

Fig. 3. Saturated solubility of CXB API, CXB–polymer PMs and SDs in the pH 6.8 PBS.

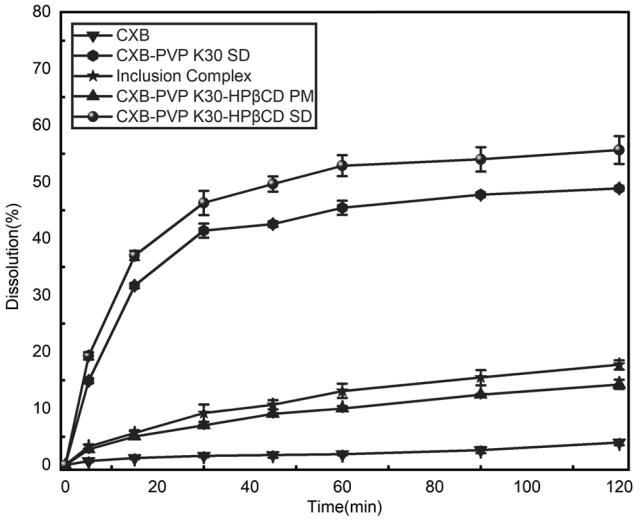

Fig. 4. *In vitro* dissolution of CXB API, CXB–polymer PM, and SDs in the pH 6.8 PBS.

which were significantly higher than the drug release of 2:1 drug–carrier ratio (38.39%). In order to facilitate the drug load along with controlling the final preparation size, a drug–carrier ratio of 1:1 was chosen for further investigation.

3.3 Saturated solubility study

Figure 3 shows saturated solubility of CXB API at the pH 6.8. PBS was only 0.718 μg/mL, which would lower therapeutic concentrations of CXB. The addition of polymer excipients into the CXB was followed by a significant improvement in saturated solubility. All the tested carriers significantly enhanced the saturated solubility of CXB. Compared with CXB API, CXB–PVP K30 PM increased saturated solubility approximately 2.1-fold. Analogously, CXB–HPβCD PM increased saturated solubility approximately 2.67-fold; the saturated solubility of ternary PM increased 4.72-fold. It is clearly visible that SDs have a better effect on the enhanced solubility than PMs. With CXB–PVP K30 SDs inclusion complex of CXB–HPβCD and CXB–PVP K30–HPβCD ternary SDs, 2.53-fold, 4.94-fold, and 6.28-fold increases in saturated solubility were observed respectively, compared with pure CXB API. These experimental results speculate that the hydrophilic structure of PVP K30 and HPβCD increased the wettability of samples in the buffer. Besides, with particle size decreasing samples of SDs also enhanced solubility [27].

3.4 *In vitro* dissolution study

As shown in Fig. 4, the *in vitro* dissolution obtained from the pure CXB API exhibited only 3.99% drug release at the end of 120 min. However, the dissolution of the inclusion complex of CXB–HPβCD was 17.73% drug release at the end of 120 min owing to the interaction between the hydrophobic portions of CXB molecules and cavities of HPβCD, which enabled enhancement of the affinities of CXB to the dissolution medium. The drug rapidly dissolved from the inclusion complex formulation [28]; then, the *in vitro* dissolution increased up to around 4.44-fold.

The *in vitro* dissolution of CXB–PVP K30 SD at the end of 120 min was measured to be 48.88%, which was around 12.25-fold over the CXB API. The in vitro dissolution behavior of solid dispersion was confirmed by XRD and FT-IR, indicating the successful hydrogen bonding between CXB

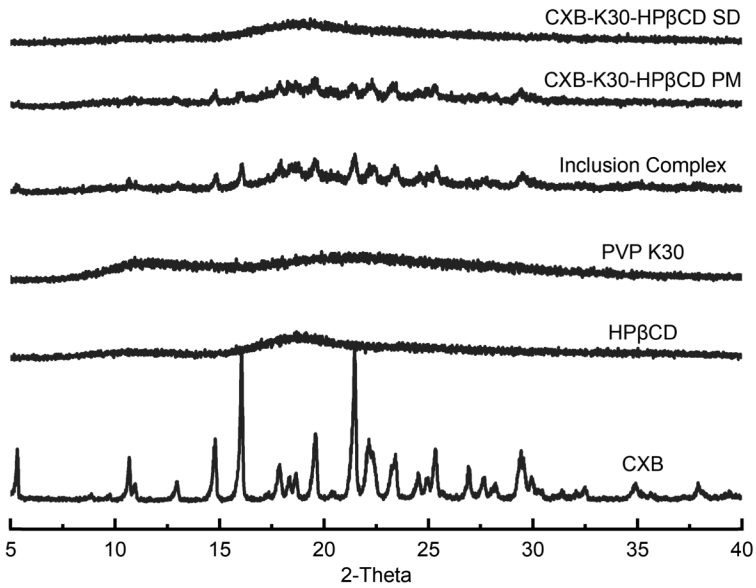

Fig. 5. x-ray diffraction (XRD) pattern of CXB API, PVP K30, HPβCD, inclusion complex, PM, and their solid dispersion samples.

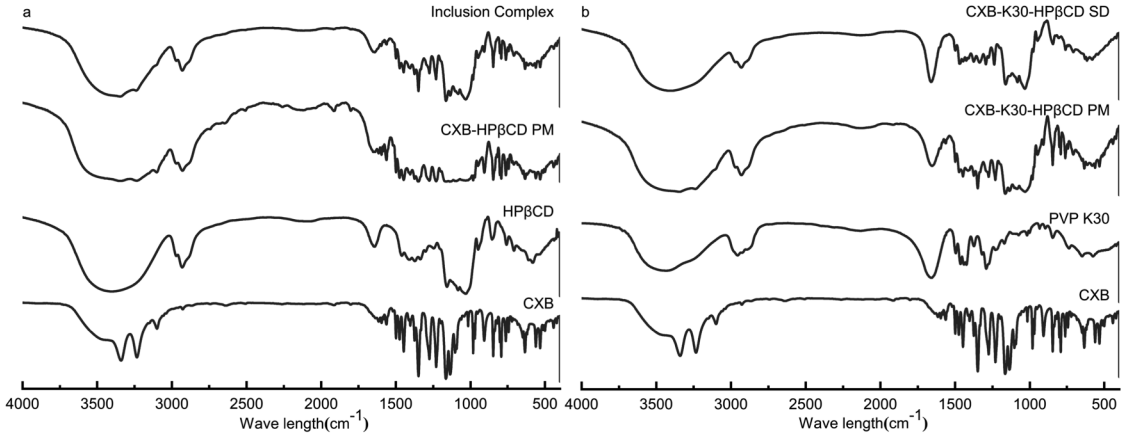

Fig. 6. (a) Fourier transform infrared spectroscopy of pure celecoxib (CXB), hydroxypropyl-β-cyclodextrin (HPβCD), CXB:HPβCD 1:4.04 (w/w) PM, CXB:HPβCD 1:4.04 (w/w) inclusion complex respectively from top to the bottom; (b) Fourier transform infrared spectroscopy of CXB, PVP K30, CXB:PVP K30:HPβCD 1:1:4.04 (w/w) PM, CXB:PVP K30:HPβCD 1:1:4.04 (w/w) SD respectively from the top to the bottom.

and PVP K30, with CXB transforming into an amorphous state in the carrier material. The *in vitro* dissolution of ternary SD at the end of 120 min was tested to be 55.64%. For comparison, under the same conditions, the drug release of PM at the end of 120 min was only 14.27%. It illustrates that the drug release *in vitro* simulated intestinal fluid can be promoted by the synergistic effect of the two carrier materials. The improvement of the *in vitro* dissolution of ternary SD not only relied on the amorphous properties of drugs, but also depended on the improvement of wettability.

3.5 x-ray diffraction studies

From the CXB diffraction patterns of Fig. 5, the diffraction peaks appear at angles of 5.039°, 10.689°, 12.946°, 16.061°, 19.547°, and 21.34° (2θ), it is indicated that CXB is a drug with high crystallinity, which was consistent with the CXB crystal structure of form III reported previously. Owing to the lack of significant diffraction peaks in patterns of PVP K30 and HPβCD, allowing the two polymers upon the formation of the amorphous form. In the presence of a CXB diffraction peak at the same angle in the CXB–HPβCD inclusion complex, CXB is generated and stabilized in crystallite as confirmed by the diminished diffraction peak, which was consistent with those reported elsewhere [29]. In fact, a superimposition of the PM's background was observed for all three tested drug loadings in the CXB–K30–HPβCD ternary system. Although the diffraction peak of CXB has completely disappeared, it confirms that CXB has been dispersed in carrier materials by the amorphous form.

3.6 FT-IR study

Figure 6 shows the infrared curves of CXB, HPβCD, and PVP K30 used in this work. For CXB, primary amine stretching vibration absorption peaks appear at 3340.8 cm^{-1}, and 3231.5 cm^{-1}, C-H of the benzene ring stretching vibration absorption peak appears at 3095.9 cm^{-1}, benzene skeleton vibration absorption peaks appear at 1500.6 cm^{-1}, and 1447.2 cm^{-1}, and O=S=O exhibits symmetric and asymmetric vibration absorption peaks at 1348.9 cm^{-1} and 1132.3 cm^{-1} respectively. In FT-IR spectra of HPβCD, the –OH stretching vibration absorption band is at 3397.96 cm^{-1}. The HPβCD spectra show stretching vibration absorption peaks at 1640.82 cm^{-1} (C=O), 1083.67 cm^{-1} (C-H), and 1032.65 cm^{-1} (C-O). The PVP K30 spectra exhibit stretching vibration absorption peaks at 2955.1 cm^{-1}, 1291.84 cm^{-1} (C-H), and 1659.18 cm^{-1} (C=O).

A simple superimposition of the CXB and HPβCD physical mixture's background was observed in the inclusion complex system. For CXB in the inclusion complex, two absorption peaks disappeared at 3340.8 cm^{-1} and 3231.5 cm^{-1}, the sharp absorption peak changed to a broad band, similar to what was previously reported, that the variation of infrared spectra confirms the formation of the inclusion complex. In this PM system, the overlapping of the absorption spectra of the three compounds is presented as the ternary physical mixture's infrared spectra. Primary amine stretching vibration absorption peaks of CXB appear at 3340.8 cm^{-1}, and 3231.5 cm^{-1}, C-H stretching vibration absorption peaks of PVP K30 are detected at 2955.1 cm^{-1}, as well as characteristic absorption peaks of HPβCD appearing at 1000 cm^{-1}. Owing to hydrogen-binding between CXB and PVP K30 in the SD, the primary amine stretching vibration absorption peaks of CXB vanished. Besides, the FT-IR spectra show reduced absorption intensity of characteristic peaks in SD, supporting the inference about the interactions of compounds, as reported previously [28].

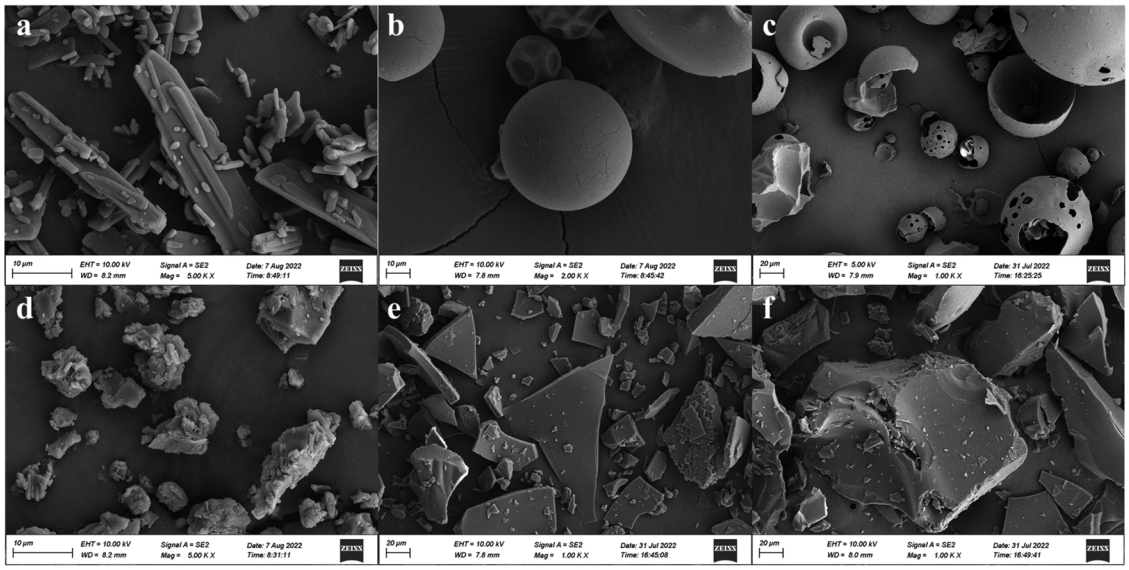

Fig. 7. Scanning electron microscopy images of different samples: (a) CXB, (b) PVP K30, (c) HPβCD, (d) CXB-HPβCD inclusion complex, (e) CXB-PVP K30 SD, and (f) CXB-PVP K30-HPβCD SD.

3.7 Scanning electron microscopy study

The form and morphology of CXB API, PVP K30, HPβCD, sample of inclusion complex, and SDs have been observed using a Zeiss scanning electron microscope. As shown in Fig. 7*a*, CXB API showed the appearance of long, needle-shaped crystals with irregular figures. An SEM image of PVP K30 (Fig. 7*b*) exhibited an irregular surface morphology with a globular shape. An SEM image of HPβCD (Fig. 7*c*) showed ball-shaped particles with a concave hole surface.

An SEM image of an inclusion complex (Fig. 7*d*) displayed patch-shaped uniform particles; nevertheless, CXB and HPβCD were observed to have inconspicuous formation of morphology. It can be speculated that an interaction between CXB and HPβCD could cause such radical changes in morphology [30]. An SEM image of Fig, 7e and f showed certain irregular sheet-like architecture in both CXB–PVP K30 binary SD and CXB-PVP K30–HPβCD ternary SD. Crystalline, long, rod-like CXB have never been observed in SDs; it demonstrated that the two formulations presented CXB in a fully amorphous state, which is in accordance with the aforementioned XRD analysis result. The significant morphological change confirmed that a novel form of state proved to have arisen between the three chemical compounds, which has been described in the aforementioned FT-IR investigation.

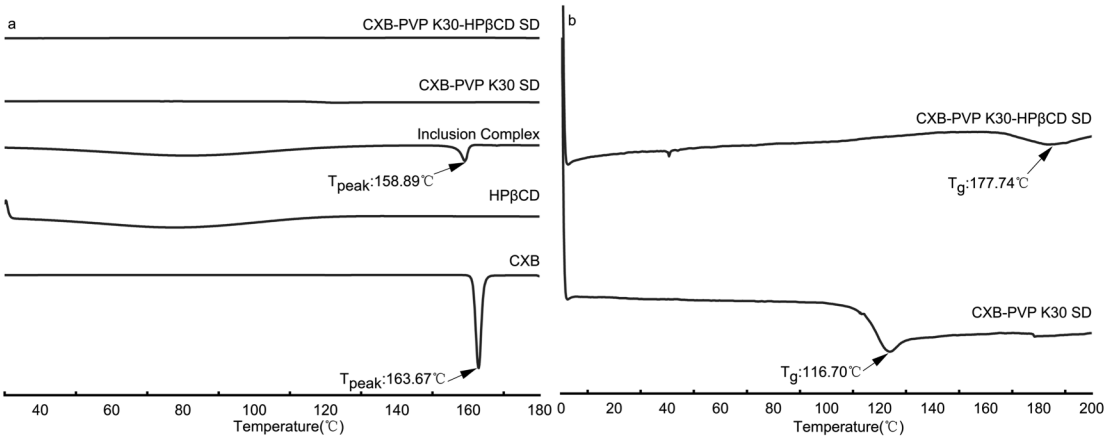

Fig. 8. Differential scanning calorimetry (DSC) thermograms of CXB API, HPβCD, inclusion complex, and SDs. (a) CXB, HPβCD, inclusion complex, CXB–PVP K30–HPβCD SD, CXB–PVP K30 SD; (b) CXB–PVP K30–HPβCD SD, and CXB–PVP K30 SD.

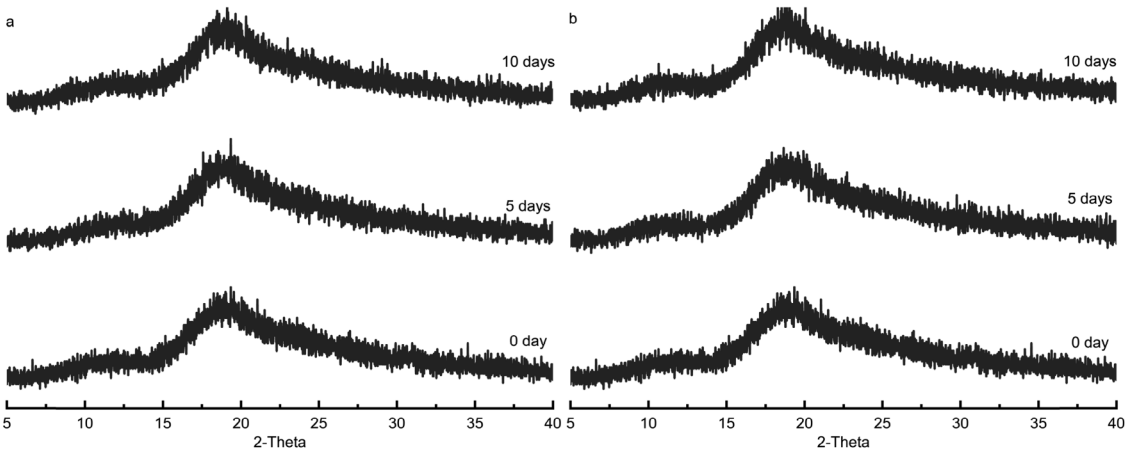

Fig. 9. x-ray diffractograms of CXB ternary SD after storage for 0 day, 5 days, and 10 days at 60°C (a), 4500 ± 500 lux light intensity (b).

3.8 Differential scanning calorimetry study

The DSC thermograms of CXB API, HPβCD, inclusion complex, and two solid dispersions are shown in Fig. 8. DSC thermograms of CXB API (Fig. 8*a*) showed a sharp melting endothermic peak at 163.67°C corresponding to the melting of CXB. A similar endothermic peak could not be detected in HPβCD, meaning that it was amorphous form in agreement with the aforementioned XRD result.

The DSC curve of the CXB–HPβCD inclusion complex showed that a melting temperature of the endothermic peak of CXB moved to 158.89°C with significantly reduced intensity compared with pure crystalline CXB. From another perspective, XRD assay confirms the reduction of crystallinity in the inclusion complex, which should also influence the endothermic peak of CXB [31]. Besides, displacement of the endothermic peak proved the presence of an interaction between CXB and HPβCD. However, in the CXB binary SD and ternary SD systems, melting endothermic peaks of CXB completely vanished, with only the glass transition temperatures (T_g) that could be observed. It is demonstrated that CXB and the polymer carriers were mixed to be homogeneous single-phase mixture systems, suggesting that the drug might be dispersed in the polymer in an amorphous form. DSC was utilized to determine the glass transition temperatures of CXB–PVP K30 SD (116.7°C) and glass transition temperatures of CXB–PVP K30–HPβCD SD (177.74°C). The T_g of CXB (around 60°C) has been measured in the pharmaceutical literature [32]. Drugs with a high glass transition temperature can effectively reduce the molecular mobility for a lagging crystallization tendency to enhance the thermostability of the solid dispersions system [33].

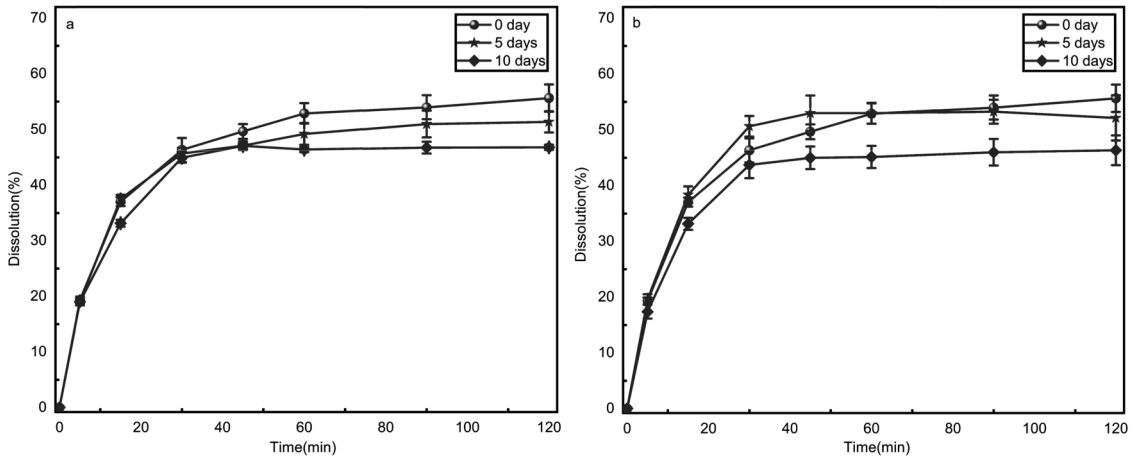

Fig. 10. Comparison of the drug-release profiles of CXB ternary SD in pH 6.8 PBS medium after storage for 0 days, 5 days, and 10 days at 60°C (a), 4500 ± 500 lux light intensity (b).

3.9 Experiment of influencing factors

The stability of the SDs issue presents many challenges in their commercialization. Section 2.4 described the storage condition of CXB ternary SD stability assays. Compared with the color and state of ternary CXB SDs at 0 days, after 10 days, the polymer SDs in the stability chamber still exhibited a white bulk powder. However, the existing state of samples under 75%±1% relative humidity has become a kind of white viscous and soft material from the white bulk powder after 5 days. It can be seen that in the presence of hydrophilia of PVP K30 and HPβCD, the appearance state of ternary SD changed to absorption of the moisture state. Owing to the softening of the samples at 75%±1% relative humidity, it was unnecessary to carry out further study.

From the diffraction patterns of Fig. 9, compared with 0 days, in the presence of the amorphous form of CXB ternary SD at 60°C and light intensity of 4500 ± 500 lux, the x-ray diffractogram at 5 days and 10 days showed a distinct lack of variation. All the results demonstrated a high degree of stability of CXB ternary SD, which should be attributed to the superior recrystallization inhibition effect of the combination of PVP K30 and HPβCD upon the accelerated test.

In vitro dissolution tests were conducted to investigate the drug release profiles from the CXB ternary SD stored under 60°C and light intensity of 4500 ± 500 lux and were compared with different samples after storage for 0 days, 5 days, and 10 days (Fig. 10). The evaluation of the 1200 min dissolution behavior of CXB ternary SD demonstrated a small reduction as storage time was prolonged. In short, from our aforementioned assays, no significant changes were observed in the XRD patterns and drug release profiles for CXB ternary SD, showing that those were able to maintain the prepared polymer formulation in a stable amorphous state for at least 10 days. Moreover, variation of the existing state of the samples, which were stored at 75% relative humidity, can infer that use of the high humidity storage condition should be avoided for CXB ternary SD prepared with PVP K30 and HPβCD.

3.10 Contact angle study

Wettability investigations of drugs usually involve the test of contact angles, as well as data on the assay indicating the degree of wetting between the solid/liquid interaction. As a rule, complete wetting occurs when the contact angle is 0°, whereas complete nonwetting would present to 180° of contact angle [34]. The results of different contact angle measurements are shown in Table 1.

TABLE 1 collects information on CXB, the water insoluble drug, whose 80° contact angle was observed. The addition of HPβCD to form the inclusion complex system is followed by the variation of the contact angle to 35.63°. By similar experimental operations, the contact angle of CXB–K30 SD and CXB–K30–HPβCD SD have turned into 36.87° and 53.37° respectively. It can be seen that with doping of the carrier materials, the hydrophilicity of the samples was improved in different degrees. From the obtained contact angle data, it could be estimated that the hydrophilicity of the ternary SD decreased in comparison with binary SD. In contrast to binary SD, it is important to note that the stronger molecular interaction of drug and two polymer carriers can lead to a comparatively large contact angle of ternary SD. Accordingly, the hydrophilicity of the carrier materials was inhibited; with lowering of ternary system hydrophilicity, the contact angle was increased. On the other hand, it could also cause a substantial difference in specimen surface property for the variation of compressibility among different samples, then the contact angle information was affected. In any SD system, after the addition of carrier material leads to the limiting step of release is switched from AIP to carrier, resulting in the improved wettability of samples.

4. CONCLUSION

In the investigation of poorly water-soluble pharmaceuticals, CXB has been widely studied as a model drug. The formulation of amorphous solid dispersions is applied to improve the solubility of nonwater soluble APIs as an effective strategy. In this study, we prepared ternary CXB SD utilizing a rotary evaporation with PVP K30 and HPβCD as carriers and characterized by SEM, XRD, FT-IR, DSC, and a contact angle meter. It shed light on the fact that CXB API interacted strongly with polymer carriers, where it is dispersed therein with internal disordered structure possess; the wettability of API was also greatly enhanced with the addition of carrier materials. Moreover, thermal characterization of the ternary

TABLE 1. Contact angle parameters (mean ± standard deviation, averaged over three samples) for celecoxib (CXB), inclusion complex, binary solid dispersions (SDs), and ternary SDs

Sample	CXB	Inclusion complex	Binary SD	Ternary SD
1	77.7°	34.9°	34.1°	54.8°
2	80.5°	34.2°	37.2°	54.5°
3	81.5°	37.8°	39.3°	50.8°
Mean value	79.9° ± 1.97°	35.63° ± 1.91°	36.87° ± 2.62°	53.37° ± 2.23°

CXB SD showed an obvious rise in glass transition temperature, suggesting the improvement of the specimen's stability by effectively reducing the molecular mobility of the amorphous SD system. Furthermore, compared with CXB API, ternary CXB SD increased solubility (PBS, pH 6.8) around 6.28-fold, and an almost 13.94-fold increase in the dissolution rate (120 min) of SD was exhibited. In this assay, the influence of temperature, light intensity, and moisture on the stability of SD samples stored under extreme conditions at the end of 5 days and 10 days was evaluated regarding their solid state and dissolution behavior. Results showed an insignificant difference in comparison with that at 0 days. Given all this, combined HPβCD/traditional carrier materials to form ternary SDs can provide a novel formulation strategy to improve the absorption of a poorly water-soluble CXB drug and facilitate in vitro dissolution. The present work affords an insight into the choice of improvement of the appropriate preparation and formulation process for fabricating stabilized, poorly soluble, CXB-loaded SDs.

Authors' contributions

Conceptualization, Lang Liu; literature research, Ting Li and Min Wen; supervision and project administration, Liqing Zhu; experimental design, Lang Liu, Ting Li, and Min Wen; conduct of the experimental work, Lang Liu and Fenfen Ouyang; writing of the first draft and data processing, Lang Liu; data analysis, Lang Liu and Fenfen Ouyang; article revision and proofreading, Guodong Zha, Libo Chen, and Xue Fu.

Funding

Natural Science Foundation of Chongqing [grant No. CSTB2022BSXM-JSX0012].

Conflicts of interest statement

The authors declare that there are no conflicts of interest.

REFERENCES

1. N. M. Davies, A. J. McLachlan, R. O. Day, et al., *Clin. Pharmacokinet.*, **38**, 225 – 242 (2000).
2. J. Li, Q. Hao, W. Cao, et al., *Cancer Manage. Res.*, **10**, 4653 – 4667 (2018).
3. N. Tołoczko-Iwaniuk, D. Dziemiańczyk-Pakieła, K. B. Nowaszewska, et al., *Curr. Drug Targets*, **20**, 302 – 315 (2019).
4. K. S. Ahmed, S. Changling, X. Shan, et al., *J. Liposome Res.*, **30**, 285 – 296 (2020).
5. A. H. Schönthal, T. C. Chen, F. M. Hofman, et al., *Expert Opin. Invest. Drugs.*, **17**, 197 – 208 (2008).
6. Ş. G. Küçükgüzel, İ. Coşkun, S. Aydın, et al., *Molecules.*, **18**, 3595 – 3614 (2013).
7. D. Clemett, K. L. Goa, *Drugs*, **59**, 957 – 980 (2000).
8. F. Norouzi, A. Jouyban, F. Martinez, et al., *Phys. Chem. Liq.*, **57**, 755 – 767 (2019).
9. X. He, M. R. Barone, P. J. Marsac, et al., *Int. J. Pharm.*, **353**, 176 – 186 (2008).
10. C. Leuner, J. Dressman, *Eur. J. Pharm. Biopharm.*, **50**, 47 – 60 (2000).
11. T. Turovsky, R. Khalfin, S. Kababya, et al., *Langmuir*, **31**, 7183 – 7192 (2015).
12. H.-I. Kim, S. Y. Park, S. J. Park, et al., *Pharmaceutics*, **10** (2018).
13. I. Hwang, V. Renuka, J.-H. Lee, et al., *Pharm. Dev. Technol.*, **25**, 525 – 534 (2020).
14. S. Mukesh, P. Joshi, A. K. Bansal, et al., *Mol. Pharm.*, **18**, 2334 – 2348 (2021).
15. T. Vasconcelos, S. Marques, J. das Neves, et al., *Adv. Drug Delivery Rev.*, **100**, 85 – 101 (2016).
16. T. Xie, L. S. Taylor, *Pharm. Res.*, **33**, 739 – 750 (2016).
17. M. Maghsoodi, A. Nokhodchi, H. Pourasghari Azar, *Pharm. Dev. Technol.*, **26**, 788 – 796 (2021).
18. K. R Berziņš, S. J. Fraser-Miller, G. F. Walker, et al., *Mol. Pharm.*, **18**, 3882 – 3893 (2021).
19. D. E. Moseson, I. D. Corum, A. Lust, et al., *The AAPS Journal*, **23**, 69 (2021).
20. E.-J. Heo, S. Y. Park, H.-I. Kim, et al., *J. Nanosci. Nanotechnol.*, **20**, 5813 – 5818 (2020).
21. A. Niederquell, E. Stoyanov, M. Kuentz, *Mol. Pharm.*, **19**, 690 – 703 (2022).
22. H. J. Kwon, E.-J. Heo, Y.-H. Kim, et al., *Pharmaceutics*, **11**(3), 136 (2019).
23. C. M. De Jongh, M. M. Verberk, C. E. T. Withagen, et al., *Contact Dermatitis*, **54**, 325 – 333 (2006).
24. K. H. Park, J. M. Choi, E. Cho, et al., *Polymers*, **10**, 111 (2018).
25. X. Yang, J. Shen, J. Liu, et al., *Crystals*, **12**, 596 (2022).
26. A. Homayouni, F. Sadeghi, A. Nokhodchi, et al., *Iran J. Basic Med. Sci.*, **17**, 322 – 331 (2014).
27. R. Ghanavati, A. Taheri, A. Homayouni, *Materials Science and Engineering: C*, **72**, 501 – 511 (2017).
28. A. Zoghbi, T. Geng, B. Wang, *AAPS PharmSciTech*, **18**, 2927 – 2935 (2017).
29. K. O. Boakye-Yiadom, S. Kesse, M. Aquib, et al., *Polym. Adv. Technol.*, **31**, 2270 – 2278 (2020).
30. V. R. Sinha, R. Anitha, S. Ghosh, et al., *Acta Pharmaceutica (Zagreb, Croatia)*, **57**, 47 – 60 (2007).
31. C. M. Hsu, S. C. Yu, F. J. Tsai, et al., *Colloids and Surfaces. B. Biointerfaces*, **180**, 68 – 74 (2019).
32. A. Homayouni, F. Sadeghi, A. Nokhodchi, et al., *Iran J. Basic Med. Sci.*, **17**, 322 – 331 (2014).
33. J. A. Baird, L. S. Taylor, *Adv. Drug Deliv. Rev.*, **64**, 396 – 421 (2012).
34. S. Verma, V. S. Rudraraju, *AAPS PharmSciTech*, **16**, 1079 – 1090 (2015).